Infrared Properties of SiO Maser Sources in Late-Type Stars

Mikako MATSUURA,[1,2] Issei YAMAMURA,[3,1] Hiroshi MURAKAMI,[1] Takashi ONAKA,[2]

Takafumi OOTSUBO,[2] Takanao TOHYA,[1,2] Yoshihiko OKAMURA,[1,4]

Minoru M. FREUND,[1,5] and Masahiro TANAKA[1]

[1] *Institute of Space and Astronautical Science (ISAS),*

3-1-1 Yoshinodai, Sagamihara, Kanagawa 229-8510

[2] *Department of Astronomy, University of Tokyo,*

7-3-1 Hongo, Bunkyo, Tokyo 113-0033

[3] *Astronomical Institute 'Anton Pannekoek', University of Amsterdam,*

Kruislaan 403, 1098 SJ, Amsterdam, the Netherlands

[4] *Department of Physics, University of Tokyo,*

7-3-1 Hongo, Bunkyo, Tokyo 113-0033

[5] *Infrared Astrophysics Branch, Code 685,*

NASA Goddard Space Flight Center, Greenbelt, MD 20771, USA

E-mail (MM): mikako@astro.isas.ac.jp

(Received ; accepted)

Abstract

Results of an SiO maser survey for the late-type stars selected by the IRTS (Infrared Telescope in Space) are presented. We have detected SiO $J = 1-0$, $v = 1$ and/or $v = 2$ lines in 27 stars out of 59 stars. The maser intensity increases with the depth of the H_2O absorption in the infrared spectra and redness of the 2.2 and 12 μm color. The column densities of the water vapor in the target stars are estimated from the depth of the water absorption in the IRTS spectra. We found that the SiO maser was detected mostly in the stars with the column density of water vapor higher than 3×10^{19}–3×10^{20} cm^{-2}. We further estimate the density of hydrogen molecules in the outer atmosphere corresponding to these column densities, obtaining 10^9–10^{10} cm^{-3} as a lower limit. These values are roughly in agreement with the critical hydrogen density predicted by models for the excitation of the SiO masers. It is possible that the SiO masers are excited in clumps with even higher than this density. The present results provide useful information on the understanding of the physical conditions of the outer atmospheres in late-type stars.

Key words: Stars: atmospheres — Stars: late-type — Radio sources: lines — Stars: long period variables — Infrared: sources

1. Introduction

One of the characteristics of the red giant stars is the possession of the atmosphere more extended than the hydrostatic case. Several kinds of molecules are formed in the extended atmosphere. Dust grains are also formed in the outermost region of the extended atmosphere, and consequently, the mass loss is accelerated by the radiation pressure on the dust grains. The extended atmosphere is thought to be generated by large pulsations of the stars. Woitke et al. (1999) showed theoretically that pulsation affects the density structure of the molecules, especially poly-atomic molecules. However, poly-atomic molecules, such as H_2O, CO_2, and SO_2, are difficult to observe from the ground because of the interference by the terrestrial atmosphere. Recent observations based on satellite missions allowed investigations of the properties of these molecules in the extended atmosphere (Tsuji et al. 1997; Justtanont et al. 1998; Ryde et al. 1999; Yamamura et al. 1999a, b). Tsuji et al. (1997) found that a layer of molecules, which the authors called a "warm molecular envelope", is also present in non-Mira variables, i.e., irregular and semi-regular variables. Pulsations of these stars are rather weak and thus it is under discussion at present if the pulsation is still responsible for the formation of the molecular layer even in non-Mira variables. Hereafter, we denote the extended atmosphere or the warm molecular envelope as an "outer atmosphere", which is the region located above the photosphere, but below the circumstellar envelope (see also Yamamura and de Jong 2000).

Matsuura et al. (1999; hereafter Paper I) have studied the water vapor absorption band at 1.9 μm based on the spectro-photometric data obtained by the Near-Infrared Spectrometer (NIRS; Noda et al.

1996) on board the Infrared Telescope in Space (IRTS; Murakami et al. 1996). The NIRS observed water vapor absorption in a large sample of stars. In the near infrared region, the water vapor is a dominant absorber in red-giants. The water vapor absorption bands are thought to arise mainly from the outer atmosphere of these stars. The strength of the water vapor absorption increases with the 2.2 and 12 μm color, $C_{12/2.2}$. This color is an indicator of the amount of dust in the inner part of the circumstellar shell. In Paper I, we suggested that the depth of the water vapor absorption represents the amount of matter in the outer atmosphere, indicating the close relation between the density of the outer atmosphere and the mass-loss rate.

SiO masers have been detected in many oxygen-rich red-giants and red-supergiants. SiO molecules are condensed into dust in the region with the temperature around $\sim$ 1000 K. SiO masers are thought to be excited in the region below the dust forming region (Nyman and Olofsson 1986), or in the outer atmosphere. VLBI observations detect SiO maser spots at 1–4 stellar radii from the central stars (Miyoshi et al. 1994; Diamond et al. 1994). The detection of these spots supports the idea proposed by Langer and Watson (1984) that the infalling wind makes inhomogeneous structures and strong SiO maser emission comes from high-density clumps. However, it is difficult to derive properties of the outer atmosphere quantitatively only from the observations of the SiO masers and to understand the circumstances for the excitation of SiO masers. Two pumping mechanisms have been proposed so far for the excitation of SiO masers; radiative pumping (e.g. Kwan and Scoville 1974; Deguchi and Iguchi 1976; Bujarrabal 1994a, b) and collisional pumping (e.g. Elitzur 1980; Doel et al. 1995). At present it is still not settled which mechanism is dominant in late-type stars.

The near- and mid-infrared observations by the IRTS provide useful information on the outer atmosphere. It is worthwhile comparing the SiO maser properties with the parameters derived from near- and mid-infrared observations by the IRTS. Previous SiO maser surveys (e.g. Allen et al. 1989; Izumiura et al. 1994) were mostly based on the IRAS Point Source Catalog (IRAS-PSC; Joint IRAS Working Group 1988). The SiO detected sources and non-detected sources are uniformly scattered in the regions of oxygen-rich stars, and are not clearly separated on the IRAS color-color diagram (Haikala 1990). The SiO maser is much more frequently detected in Mira variables than in other variable types. Only a few semi-regular and irregular variables exhibit the SiO maser activity. The non-Mira SiO maser sources usually have a visual amplitude larger than 2.5 mag (Alcolea et al. 1990), which is comparable to Mira variables. Thus it is suggested that SiO maser excitation is related to the stellar pulsation because stars with a larger visual amplitude are expected to have stronger pulsation. Alcolea et al. (1990) suggested that fewer detections of the SiO maser in semi-regular variables indicates less developed outer atmosphere in these stars because the pulsation of semi-regulars is weaker than that of Miras.

In this paper, we report the results of an SiO maser survey in a sample of the IRTS point sources. The IRTS provided a large number of stellar spectra in near- and mid-infrared regions, unaffected by the terrestrial atmosphere. The infrared colors and the strength of the water absorption are compared with the SiO maser intensity. We will discuss the conditions for the excitation of the SiO masers.

2. Observations

We made observations of the SiO masers with the 45-m telescope at Nobeyama Radio Observatory from May 20 to 25, and from June 10 to 12, 1998. We simultaneously observed three SiO maser lines, $J = 1-0, v = 1$ (43.1220 GHz), $J = 1-0, v = 2$ (42.8205 GHz), and $J = 2-1, v = 1$ (86.2434 GHz). Two cooled SIS receivers (S40 for 43 GHz, and S100 for 86 GHz) were used with acousto-optical spectrometers (AOS's). Each AOS covers 40 MHz with a resolution of 37 kHz. The velocity coverage is about ± 140 km s^{-1} for the $J = 1-0$ lines, and about ± 70 km s^{-1} for the $J = 2-1$ line, respectively. The overall system temperature at 43 GHz was typically 150–250 K with the worst case of 900K, depending on the weather and the telescope elevation. The $J = 2-1$ line was observed only when the conditions were appropriate, and the overall system temperature ranged between 300 and 450 K. The half-power beam width of the telescope is 40 arcsec at 43 GHz and 18 arcsec at 86 GHz, respectively. Conversion factors from antenna temperature ($T_{\rm a}^*$ in K) to flux density (Jy) are 2.0 Jy K^{-1} at 43 GHz, and 2.6 Jy K^{-1} at 86 GHz.

The target stars were selected from a preliminary list of the IRTS point sources, whose spectra were obtained by both the Mid-Infrared Spectrometer (MIRS; Roellig et al. 1996), and the NIRS. The selection criteria are : (1) The flux is approximately larger than 10 Jy at 10 μm and larger than 1 Jy at

2.2 μm. To get a wide coverage of different infrared colors and water indices, we also include some stars with flux below 10 Jy at 10 μm; (2) The spectrum shows the characteristics of an oxygen-rich star (c.f. Yamamura et al. 1997). Carbon-rich stars and S-type stars in the catalogues (Stephenson 1984, 1989) are excluded; (3) The star has an identification in the IRAS-PSC. In the present study, we include some stars near the galactic plane, which were not included in Paper I. The positions of the stars are taken from the IRAS-PSC, the General Catalogues of Variable Stars (GCVS; Kholopov et al. 1988), the Smithsonian Astrophysical Observatory Star Catalog (SAO; Smithsonian Institution 1966), and in a few cases from other catalogues.

3. Results

The SiO $J = 1-0, v = 1$ and/or $v = 2$ maser lines were detected in 27 stars out of 59 target stars. The infrared properties of detected sources and non-detected sources are listed in tables 1 and 2. The results of SiO observations are presented in tables 3 and 4. The spectra of the SiO masers are shown in figure 1. The infrared colors $C_{2.2/1.7}$ and $C_{12/2.2}$, and the water index $I_{\mathrm{H_2O}}$ in table 1 and 2 are defined by:

$$C_{2.2/1.7} = \log(F_{2.2}/F_{1.7}), \tag{1}$$

$$C_{12/2.2} = \log(F_{12}/F_{2.2}), \tag{2}$$

and

$$I_{\mathrm{H_2O}} = \log(F_{\mathrm{cont.}}/F_{1.9}), \tag{3}$$

where $F_{2.2}$, $F_{1.7}$, $F_{1.9}$ are the IRTS/NIRS flux densities in units of Jy at the 2.2, 1.7 and 1.9 μm channels, respectively. F_{cont} is the continuum flux level at 1.9 μm, which is calculated by linear interpolation between $F_{1.7}$ and $F_{2.2}$. F_{12} is the IRAS 12 μm flux. $C_{2.2/1.7}$ is an indicator of spectral types for stars earlier than M6 (see Paper I). In the following discussion, we use the peak intensity of $J = 1-0, v = 2$ to represent the strength of the SiO masers of each star. The integrated intensity has almost a linear relation with the peak intensity. The relation between the peak intensities of $J = 1-0, v = 2$ and $J = 1-0, v = 1$ lines is also mostly linear.

One irregular variable, TU Lyr (= IRAS 18186 + 3143), shows a strong $J = 2 - 1, v = 1$ maser intensity, while the $J = 1 - 0, v = 1$ and $v = 2$ lines are rather week. This object has an unusually broad line-width of about 20 km s^{-1} compared to the line-widths less than 10 km s^{-1} for other stars.

4. Detection Rate of the SiO Masers and the Infrared Properties

4.1. IRAS color-color diagram

The distribution of our sample on the IRAS color-color diagram is shown in figure 2. All the sampled stars have good IRAS flux quality at 12 and 25 μm. Four stars with low quality at the 60 μm band are not plotted in figure 2. The division on the color-color diagram is taken from van der Veen and Habing (1988). The sampled stars are mostly distributed in region II and IIIa, which are the regions for oxygen-rich AGB stars with a low mass-loss rate of the order of 10^{-7} $M_\odot$ yr^{-1} (van der Veen and Habing 1988). Several stars are located in region VII, which is the region for carbon stars. However, the near-infrared spectra confirm their oxygen-rich nature. 'Detection' in figure 2 indicates either $J = 1 - 0, v = 1$ or $J = 1 - 0, v = 2$ lines are detected in that star. No clear distinction is seen between the detected sources and the non-detected sources on the IRAS color-color diagram. This result is consistent with previous studies (e.g. Haikala 1990).

4.2. Near-infrared color and water index

One of the purposes of this survey is to search for the SiO masers in early M-type stars with water absorption reported in Paper I. These stars are supposed to have developed an extended atmosphere already among the early M-type stars observed by the NIRS, and thus, SiO masers might be excited. We observed two stars in this category visible from Nobeyama, AK Cap (M2) and IRAS 20073−1041 (=SAO 163310, M3). However, SiO masers were not detected in both stars.

Figure 3 shows the distribution of the observed sources on the $I_{\mathrm{H_2O}}$ and $C_{2.2/1.7}$ diagram. For reference, we plot several lines taken from figure 3 of Paper I. Three lines at the left bottom corner indicate the estimated zero level of the $I_{\mathrm{H_2O}}$ and $C_{2.2/1.7}$ relation for stars without H_2O absorption, and the $\pm 2\sigma$ deviations from that level. Stars above $+2\sigma$ line clearly exhibit water absorption (see figure 4 in Paper I).

$C_{2.2/1.7}$ is an indicator of spectral types for stars earlier than M6. Stars bluer than $C_{2.2/1.7} < -0.085$ (vertical line) are expected to have spectral types earlier than M6. One M6 star, IRAS 19461+0334 (WX Aql), which was not included in Paper I, is actually located leftward of this vertical line, but this will not affect our conclusions in this paper. In figure 3, a clear separation is seen between the SiO detected sources and the SiO non-detected sources. SiO masers are detected in stars with strong H_2O absorption (I_{H_2O} is approximately larger than 0.1). In addition, stars in the region of I_{H_2O} larger than ~ 0.1 are mostly Mira variables when their variable types are known. SiO masers are seldom detected in non-Mira variables (see Habing 1996). The present study confirms the same trend. The numbers of the SiO maser detected sources and non-detected sources for different variable types are summarized in table 5. SiO masers are detected with a high probability in Mira variables, while they are hardly detected in SRs and Lbs.

5. The Relation between SiO Maser Intensity and Infrared Parameters

5.1. Near- and mid-infrared color

The infrared color $K - [12]$ is considered as an indicator of mass-loss rate for Mira variables (Whitelock et al. 1994; Le Sidaner and Le Bertre 1996). We use $C_{12/2.2}$ instead of $K - [12]$, because the $F_{2.2}$ band represents the continuum level in K. The relation between the SiO maser intensity and the $C_{12/2.2}$ is shown in figure 4. We plot the SiO maser intensity divided by $F_{2.2}$. We implicitly assume that the intrinsic 2.2 μm band luminosities of the sample stars are similar, and that the extinction by circumstellar dust is small in the 2.2 μm band, except for a few extremely red stars. In figure 4, the SiO maser intensity seems to correlate with $C_{12/2.2}$ in the color range $C_{12/2.2} < 0.5$. Thus SiO maser intensity increases with mass-loss rate. The color $C_{12/2.2} = +0.5$ corresponds to a dust mass-loss rate of approximately 7×10^{-9} $M_\odot$ yr^{-1}. Here we use the equations in Le Sidaner and Le Bertre (1993, 1996) and the zero magnitude flux of $F_{2.2}$ is equal to 625 Jy (Cohen 1997). We assume the inner radius of the dust shell of 2.5×10^{14} cm and the expanding velocity of 10 km s^{-1}.

Nyman and Olofsson (1986) suggested that the SiO maser intensity does not correlate with mass-loss rate. They use a mass-loss rate calculated from CO $J = 1-0$ thermal emission. The CO emission is usually dominated by the molecules in the outer region of the circumstellar envelope and it represents a mass-loss rate averaged over the past thousands years. On the other hand, $K-[12]$ or $C_{12/2.2}$ represents emission from hot dust in the inner envelope and thus these colors indicate a recent mass-loss rate of the star. Since SiO masers are thought to be excited just below the dust forming region, it is likely that the SiO maser intensity correlates better with $C_{12/2.2}$ than the CO emission.

5.2. Water index

The SiO maser intensity is shown as a function of $I_{\mathrm{H_2O}}$ in figure 5. In general, the SiO maser intensity among the detected stars increases with $I_{\mathrm{H_2O}}$, but the scatter is large. The large scatter might come from the time variation of the water absorption and the SiO maser intensity. In Mira variables, the water absorption depth changes from phase to phase (Hyland 1974), and the column density of water changes by a factor of 10 (Hinkle and Barnes 1979). The SiO maser intensity also varies by up to a factor of 10 (Nyman and Olofsson 1986; Alcolea et al. 1999). The variabilities in both quantities might obscure the relation between the water index and the SiO maser intensity.

6. Discussion

Figures 3 and 5 indicate that the sources showing the SiO maser lines have $I_{\mathrm{H_2O}}$ larger than ~ 0.1 and they are mostly Mira variables. Since the water index, $I_{\mathrm{H_2O}}$, roughly indicates the column density of water molecules in the outer atmosphere, it is suggested that water column density is systematically different between the SiO maser detected stars and non-detected stars, and also between Miras and non-Miras. The SiO maser is known to be detected quite often in Mira variables, while it is hardly detected in non-Miras (see Habing 1996). Alcolea et al. (1990) interpreted it in terms of the idea that the outer atmosphere is more ‘developed’ in Miras than in non-Miras. Miras have stronger pulsation than non-Miras. Stronger pulsation will lift up more matter from the photosphere into the outer atmosphere, leading to the higher density and thus higher column density of the molecules. Our results of the relation with $I_{\mathrm{H_2O}}$ indicate that the high detection rate of the SiO maser in Miras is related to the high column density in the outer atmosphere.

The column densities of water molecules have been measured for several stars. In table 6, we summarize the results of near-infrared observations of the H_2O bands reported in Paper I and other literatures. In Paper I we estimated the column density (N) and the excitation temperature ($T_{\rm ex}$) of the water molecules in two early M-type stars, AK Cap and V Hor. The water spectra of these stars were fitted by synthesized spectra using a plane-parallel model. We apply the same method for SAO 163310 (M3) and the results are indicated in table 6. The column densities of these stars are as uncertain as one order of the magnitude due to the low spectral resolution of the IRTS/NIRS ($\lambda/\Delta\lambda \approx 15$). These three early M-type stars show relatively strong H_2O absorption bands among the stars with similar spectral types (Paper I). Therefore, the resultant column densities are rather high compared to the other stars of similar types. Hinkle and Barnes (1979) and Yamamura et al. (1999b) interpreted the observations of the water bands in the Mira variables in terms of two molecular layers. We list the parameters of both layers in table 6. Hinkle and Barnes (1979) analyzed high-resolution spectra ($\lambda/\Delta\lambda$ = a few tens of thousands) of the Mira variable, R Leo, at K and H bands, and found two radial velocity components of water lines. One component has an excitation temperature of 1750 K and the other component about 1150 K. Yamamura et al. (1999b) fitted the water bands taken by the ISO/SWS (Short-Wavelength Spectrometer) in o Cet and Z Cas using their 'slab' model consisting of two water vapor layers. They stated that the layer with $T_{\rm ex}$ = 2000 K should be as large as 2 $R_\star$ in order to reproduce the emission band seen at 3.5–4.0 μm in o Cet. The cool layer is responsible for the absorption feature between 2.5 and 3.5 μm. In the case of Z Cas, the hot layer is located around 1 $R_\star$ and both hot and cool layers contribute to absorption. Hinkle and Barnes (1979) mention that the 1750 K layer is located near the photosphere. This layer may be identical to the 2000 K layer at 1–2 $R_\star$ in Yamamura et al. (1999b). The cool layer with $T_{\rm ex}$ = 1200–1400 K of Miras in Yamamura et al. (1999b) is as large as 2 $R_\star$ or larger. Tsuji et al. (1997) also showed that the layer with an excitation temperature of about 1000 K is located at $\sim$ 2 $R_\star$ in irregular and semi-regular variables. We note that according to the 'slab' model, when the water layer with $T_{\rm ex}$ = 1500 K is extended to 3 $R_\star$, or the layer with $T_{\rm ex}$ = 1000 K to 5 $R_\star$, the water spectra should be observed in emission around 2.7 μm, which is not the case for the present sample. We suppose that the layers with temperatures between 1000 and 1500 K in the stars in table 6 lie around

$2\ R_\star$.

Table 6 shows that the stars with the SiO maser have the water column density higher than 3×10^{19}–3×10^{20} cm^{-2}, and non-detected stars have column density lower than 5×10^{19} cm^{-2}. The column densities in table 6 vary by more than one order of magnitude among the stars. It is difficult to extend the water layer with the excitation temperature above 1000 K in such a large scale as discussed above. Thus, the large difference in the water column density should be attributed to the difference in the water density in the stars. The density of the hydrogen molecules in the outer atmosphere can be estimated by dividing the water column densities by H_2O abundance and the thickness of the layer. Analysis based on the spherical model should be required to make more accurate estimate, but in this paper we use the numbers derived from a slab model for a rough estimate. The density is probably inhomogeneous in the outer atmosphere and the SiO maser might be excited in the clumps with high-density in the outer atmosphere as suggested by Langer and Watson (1984). We try to estimate a lower limit of the density. The H_2O abundance ratio calculated with thermal equilibrium is in the order of 10^{-4} (Tsuji 1964). It depends on the abundance in the atmosphere. As representative value, we adopt relatively large H_2O abundance of Barlow et al. (1996), $H_2O/H_2 = 8 \times 10^{-4}$. We assume that the size of the H_2O layer is $1\ R_\star$ in line of sight, based on the estimated location of the water layer of 1000–1500 K at $\sim 2\ R_\star$. The stellar radius $R_\star$ is between 3×10^{13} and 5×10^{13} cm in Mira variables (Tuthill et al. 1993; Tuthill et al. 1994), and is estimated as 3×10^{13} cm for a semi-regular variable using Tuthill, Haniff and Baldwin (1999) and Hipparcos and Tycho Catalogues (1997). We adopt 5×10^{13} cm for the stellar radius. With these values we obtain 10^9–10^{10} cm^{-3} for a lower limit of the molecular hydrogen density corresponding to the water column density of 3×10^{19}–3×10^{20} cm^{-2}.

The estimated number of $n(H_2) = 10^9$–10^{10} cm^{-3} is roughly in agreement with the hydrogen density where recent theoretical works predict that the maser intensity increases drastically (Bujarrabal 1994a; Doel et al. 1995). Bujarrabal (1994a) showed that the SiO maser intensity increases by four orders of magnitudes at the hydrogen densities of $n(H_2) \sim 10^8$–10^9 cm^{-3}. Doel et al. (1995) also showed that the maser gain coefficient (gain per unit amplification path length) increases steeply at $n(H_2) \sim 5 \times 10^9$ cm^{-3}. Therefore, the probability of the SiO maser detection may be prescribed by the critical density of about 10^9–10^{10} cm^{-3}. However, the critical density at the 'spots' where the SiO maser is excited may be even higher if the maser is excited in high-density clumps (Langer and Watson 1984).

Figure 4 shows the correlation between $C_{12/2.2}$ and the SiO maser intensity, which implies the relation between the density and the excitation of the SiO masers. $C_{12/2.2}$ is a measure of the dust mass-loss rate in the innermost region of the circumstellar envelope. The mass-loss rate in this region is expected to increase with the density in the outer atmosphere. Therefore, the correlation between $C_{12/2.2}$ and SiO maser intensity also implies that the maser excitation is related to the density in the outer atmosphere.

Apart from the density, there might be other possibilities which affect the amplification of the SiO masers and lead to the dependence of detection rate on the variable types. For example, Hinkle, Lebzelter and Scharlach (1997) show that the amplitude of velocity variation depends on the amplitude of visual magnitudes. The velocity structure might vary depending on the strength of pulsation, which could result in the coherent path length for maser amplification. Further observational studies in the infrared region with high resolution observations are required to investigate the effects of velocity structure on the maser excitation.

7. Summary

The IRTS provided a large number of stellar spectra without the interference from the terrestrial atmosphere. These data enable us a systematic study of the relation between the SiO maser excitation and the conditions of the outer atmosphere. The IRTS measured the water index $I_{\mathrm{H_2O}}$ in red giants, which is an indicator of the water column density in the outer atmosphere. In 59 stars selected from the objects observed by the IRTS, the SiO maser lines were detected in 27 stars. Stars with deep water absorption ($I_{\mathrm{H_2O}}$ larger than ~ 0.1) mostly show the SiO maser lines, and they are mostly Mira variables among those with known spectral type. The SiO maser intensity is found to increase with the color $C_{12/2.2}$ and $I_{\mathrm{H_2O}}$.

Stars with $I_{\mathrm{H_2O}}$ larger than ~ 0.1 mostly show SiO masers, and the stars with SiO maser activity have the water column density higher than 3×10^{19}–3×10^{20} cm^{-2}, while non-detected stars show smaller than 5×10^{19} cm^{-2}. A lower limit of the molecular hydrogen density corresponding to the water column density is estimated as 10^9–10^{10} cm^{-3}. This number is roughly comparable with the critical gas density predicted by the models, where the SiO masers are excited (Bujarrabal 1994a; Doel et al. 1995). If the SiO masers are excited in high-density clumps (Langer and Watson 1984), the critical density would be even higher than the values we derived here.

The color $C_{12/2.2}$ well-correlates with the SiO maser intensities. $C_{12/2.2}$ is probably influenced by the density of the outer atmosphere. The relation $C_{12/2.2}$ with the SiO masers also suggests that the density of the outer atmosphere is one of the key parameters in the SiO maser excitation.

We would like to thank the staff of Nobeyama Radio Observatory for their supports. We also appreciate Drs. S. Deguchi, H. Izumiura, and T. Fujii for their suggestions for the observations. M.M. thanks the Research Fellowships of the Japan Society for the Promotion of Science for the Young Scientists. I.Y. acknowledges the financial support from a NWO PIONIER grant.

References

Alcolea J., Bujarrabal V., Gómez-González J. 1990, A&A 231, 431

Alcolea J, Pardo J.R., Bujarrabal V., Bachiller R., Barcia A., Colomer F., Gallego J.D., Gómez-González J. et al. 1999 A&AS 139, 461

Allen D.A., Hall P.J., Norris R.P., Troup E.R., Wark R.M., Wright A.E. 1989, MNRAS 236, 363

Barlow M.J., Nguyen-Q-Rieu, Truong-Bach, Cernicharo J., Gonzalez-Alfonso E., Liu X.W., Cox P., Sylvester R.J. et al. 1996, A&A 315, L241

Buhl D., Snyder L.E., Lovas F.J., Johnson D.R. 1974, ApJ 192, L97

Bujarrabal V. 1994a, A&A 285, 953

Bujarrabal V. 1994b, A&A 285, 971

Cohen M. 1997 in Proceedings for 'Diffuse Infrared Radiation and the IRTS', ASP Conference Series, vol.124, ed., H. Okuda, T. Matsumoto, T.L. Roellig, p. 61

Deguchi S., Iguchi T. 1976, PASJ 28, 307

Diamond P.J., Kemball A.J., Junor W., Zensus A., Benson J., Dhawan V. 1994, ApJ 430, L61

Doel R.C., Gray M.D., Humphreys E.M.L., Braithwaite M.F., Field D. 1995, A&A 302, 797

Elitzur M. 1980, ApJ 240, 553

Herpin F., Baudry A., Alcolea J., Cernicharo J. 1998, A&A 334, 1037

Habing H.J. 1996, A&ARv 7, 97

Heske E. 1989, A&AS 208, 77

Haikala L.K. 1990 A&AS 85, 875

Hinkle K.H., Barnes T.G. 1979, ApJ 227, 923

Hinkle K.H., Lebzelter T., Scharlach W.W.G. 1997 AJ 114, 2686

The Hipparcos and Tycho Catalogue 1997, ESA

Hyland A.R., 1974, Highlights of Astronomy, vol. 3, 307, IAU

Justtanont K., Feuchtgruber H., de Jong T., Cami J., Waters L.B.F.M., Yamamura I., Onaka T. 1998, A&A 330, L17

IRAS Point Source Catalog 1988, Joint IRAS Working Group, Washington DC. (IRAS-PSC)

Izumiura H., Deguchi S., Hashimoto O., Nakada Y., Onaka T., Ono T. Ukita N., Yamamura I. 1994, ApJ 437, 419

Kholopov P.N., Samus N.N., Frolov M.S., Goranskij V.P., Gorynya N.A., Kireeva N.N., Kukarkina N.P., Kurochkin N.E. et al. 1988, 'General Catalogue of Variable Stars, 4th Ed.' (Nauka Publishing House, Moscow) (GCVS)

Kwan J., Scoville N. 1974, ApJ 194, L97

Langer S.H. & Watson W.D. 1984, 284, 751

Le Sidaner P., Le Bertre T. 1993, A&A 278, 167

Le Sidaner P., Le Bertre T. 1996, A&A 314, 896

Matsuura M., Yamamura I., Murakami H., Freund M.M., Tanaka M. 1999, A&A 348, 579 (Paper I)

Miyoshi M., Matsumoto K., Kameno S., Takaba H., Iwata T. 1994, Nature 371, 395

Murakami H., Freund M.M., Ganga K., Guo H.F., Hirao T., Hiromoto N., Kawada M., Lange E.A. et al. 1996, PASJ 48, L41

Noda M., Matsumoto T., Murakami H., Kawada M., Tanaka M., Matsuura S., Guo H.F. 1996, SPIE

2817, 248

Nyman L.Å., Olofsson H. 1986, A&A 158, 67

Roellig T., Mochizuki K., Onaka T., Tanabe T., Yamamura I., Yuen L.M. 1996, SPIE 2817, 258

Ryde N., Eriksson K., Gustafson B. 1999, A&A 341, 579

Smithsonian Astrophysical Observatory Star catalog 1966, Smithsonian Institution, Washington DC. (SAO)

Spencer J.H., Winnberg A., Olnon F.M., Schwartz P.R., Matthews H.E., Downes D. 1981 AJ, 86, 329

Stephenson C.B. 1984, 'General Catalog of S Stars', 2nd ed., Publication of Warner & Swasey Observatory

Stephenson C.B. 1989, 'General Catalog of Cool Galactic Carbon Stars', 2nd ed., Publication of Warner & Swasey Observatory

Tuthill P.G., Haniff C.A., Baldwin J.E. 1993, in Proceedings for 'Very High Angular Resolution Imaging', IAU Symp.158 ed., J.G. Robertson, W.J. Tango, p. 395

Tuthill P.G., Haniff C.A., Baldwin J.E., Feast M.W. 1994, MNRAS 266, 745

Tuthill P.G., Haniff C.A., Baldwin J.E. 1999, MNRAS 306, 353

Tsuji T. 1964 Ann. Tokyo Astr. Obs., 9, 1

Tsuji T., Ohnaka K., Aoki W., Yamamura I. 1997, A&A 320, L1

Van der Veen W.E.C.J, Habing H.J. 1988, A&A 194, 125

Whitelock P., Menzies J., Feast M., Marang F., Carter B., Roberts G., Catchpole R., Chapman J. 1994, MNRAS 267, 711

Woitke P., Helling Ch., Winters J.M., Jeong K.S. 1999, A&A 348, L17

Yamamura I. and the IRTS Team 1997 in Proceedings for 'Diffuse Infrared Radiation and the IRTS', ASP Conference Series, vol.124, ed., H. Okuda, T. Matsumoto, T.L. Roellig, p. 72

Yamamura I., de Jong T., Onaka T., Cami J., Waters L.B.F.M. 1999a, A&A 341, L9

Yamamura I., de Jong T., Cami J. 1999b, A&A 348, L55

Yamamura I., de Jong T. 2000, ESA SP-456, in press

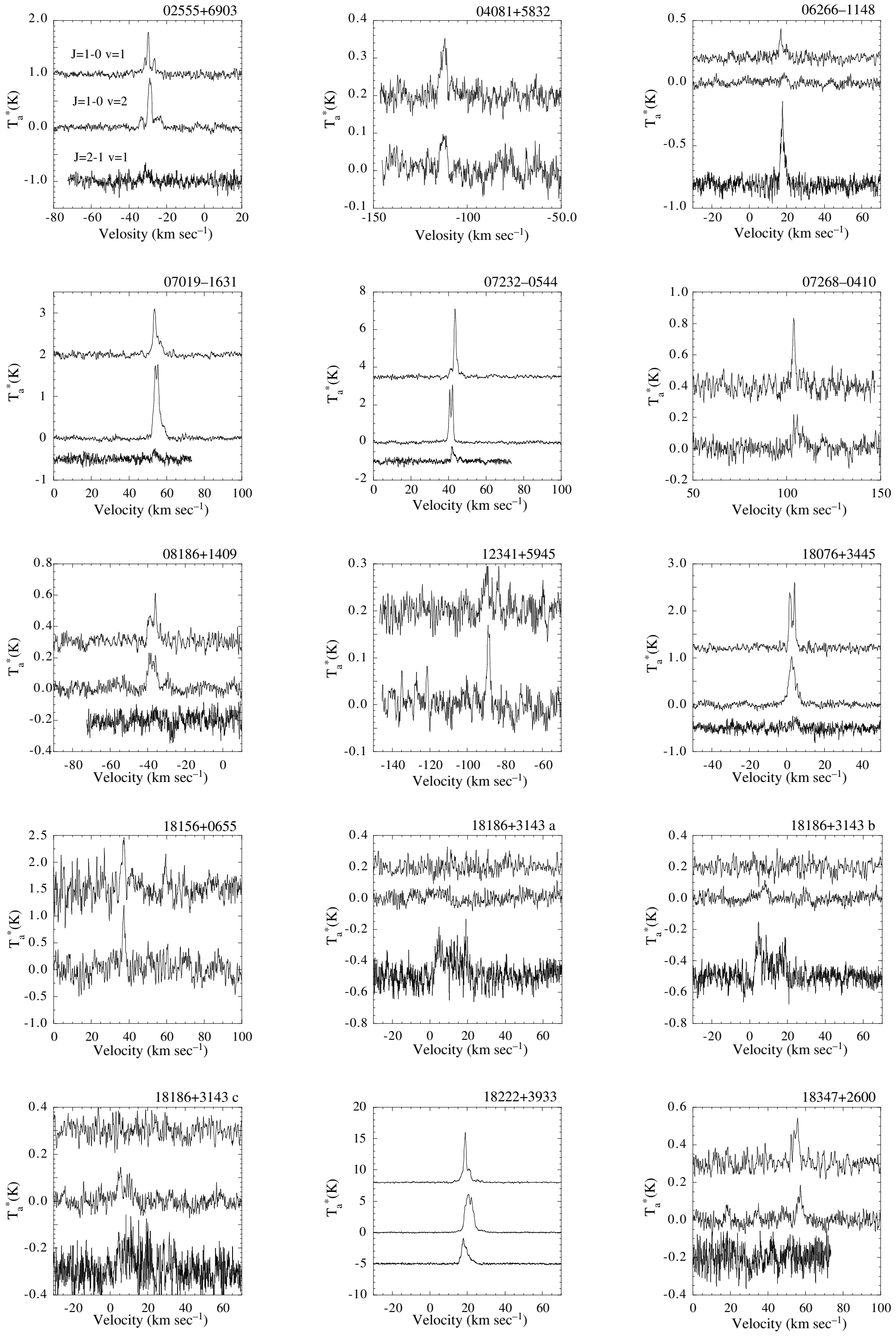

Fig.1.a. SiO maser spectra of detected sources are shown. From top to bottom, spectra indicate $J = 1-0, v=1$; $J=1-0, v=2$; and $J=2-1, v=1$ lines. When $J=2-1, v=1$ line was not observed, only two $J=1-0$ spectra are presented. IRAS $18186+3143$ was observed three times, and every spectra are plotted.

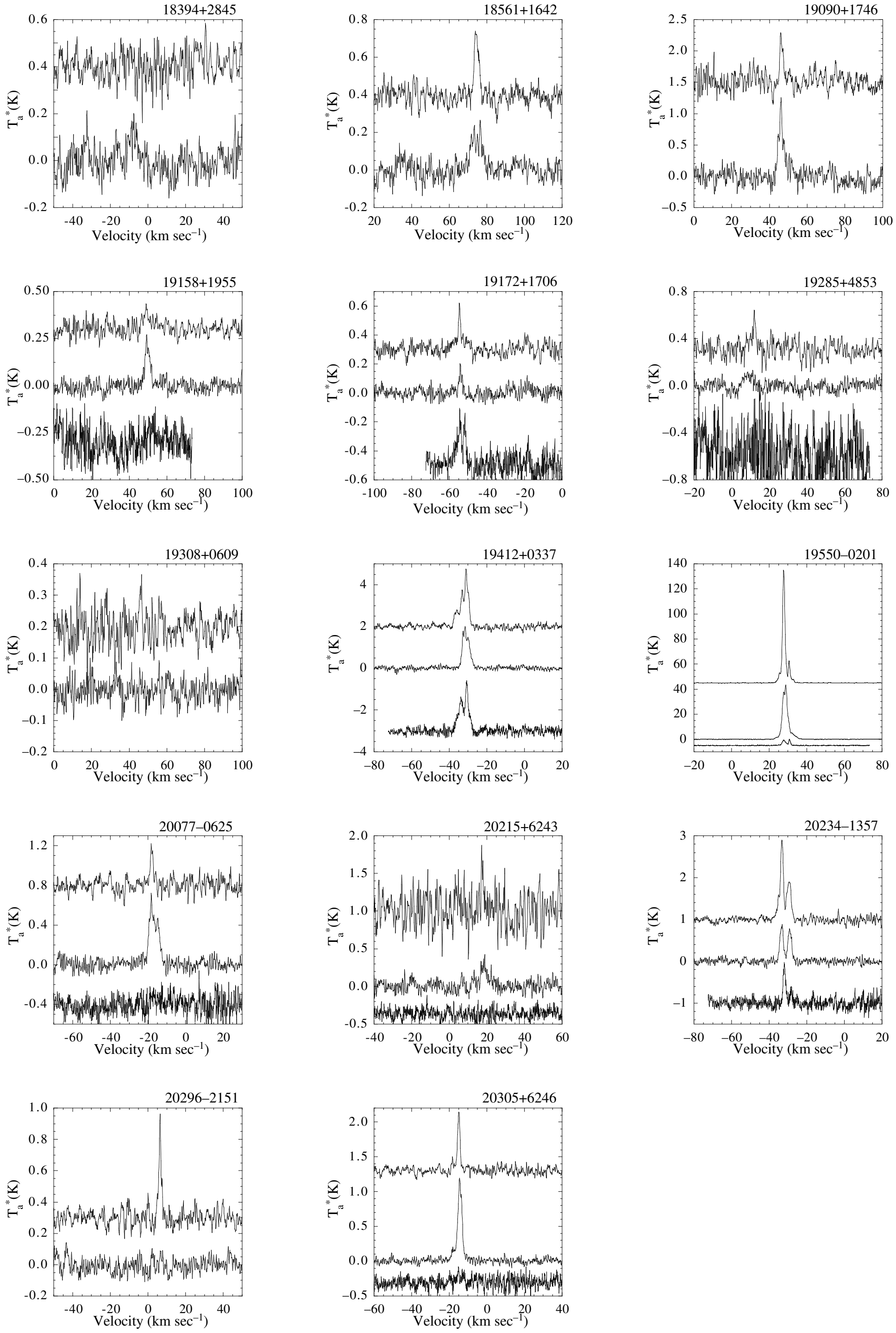

Fig.1.b. Same as figure 1.a.

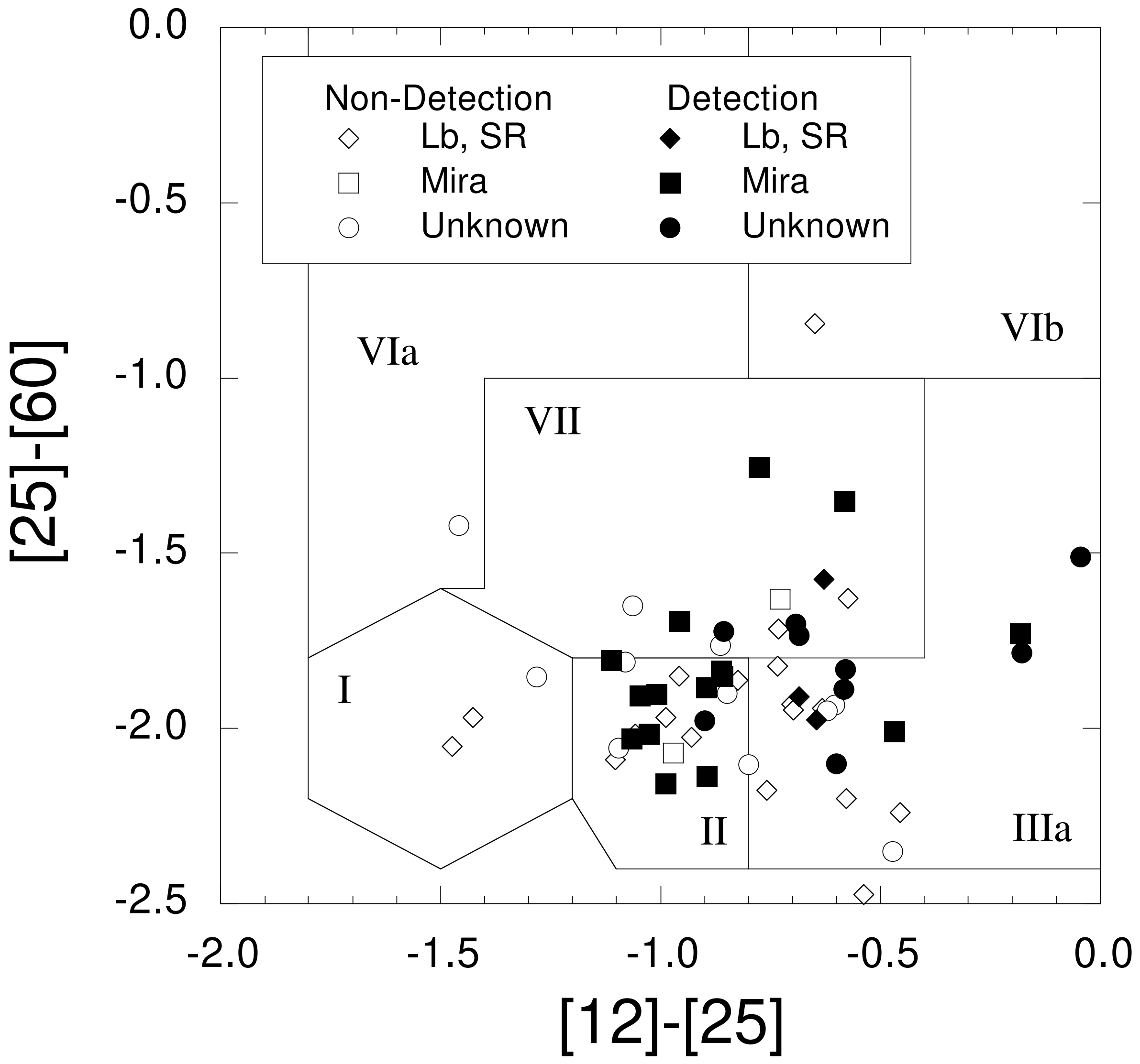

Fig.2. Observed stars of our SiO maser survey are plotted on the IRAS color-color diagram. The division of the regions comes from van der Veen & Habing (1988). The SiO detected stars are not well separated from the non-detected stars.

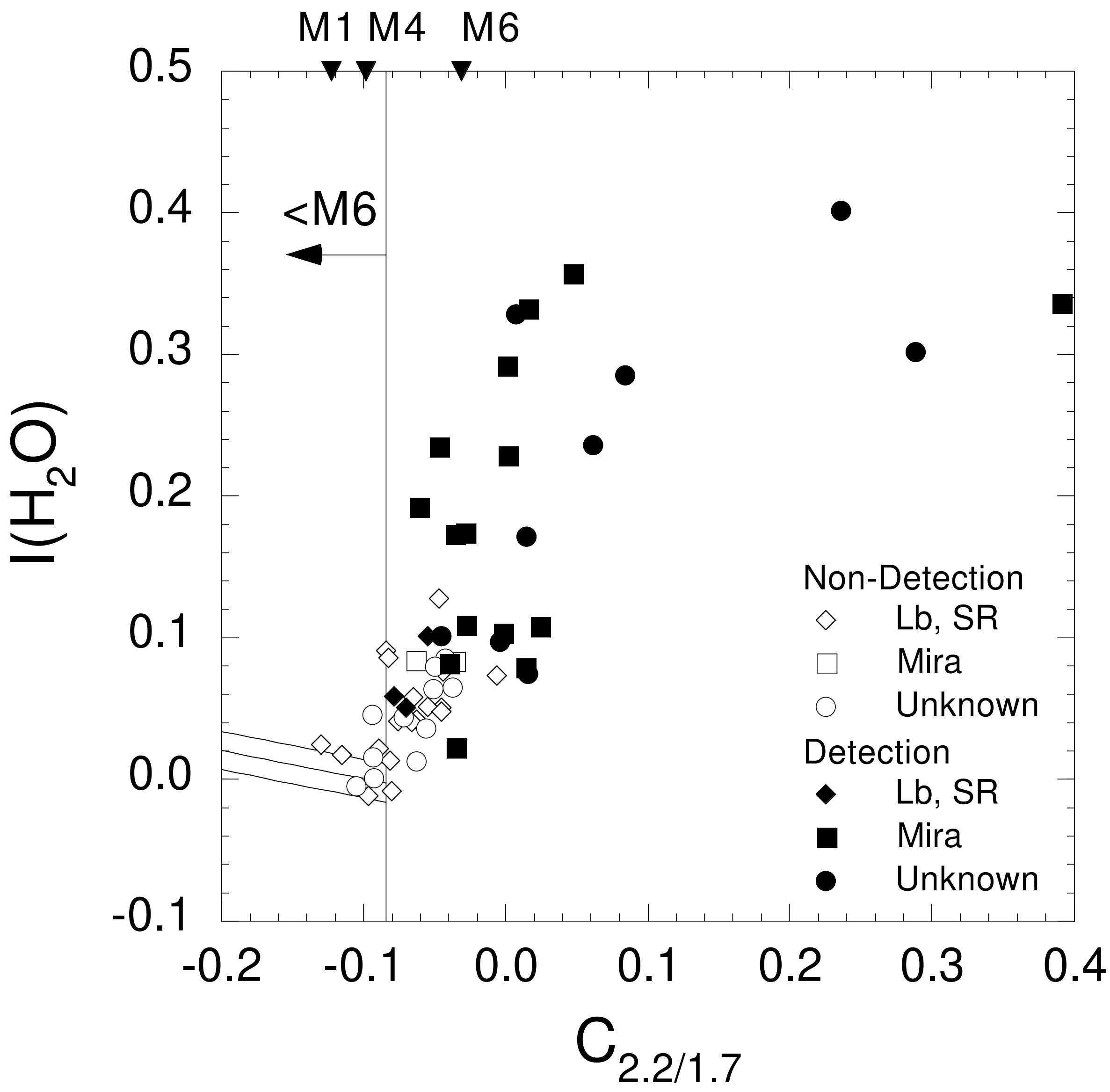

Fig.3. The water index $I_{\mathrm{H_2O}}$ is plotted as a function of $C_{2.2/1.7}$. The lines are from Paper I (see text). Symbols indicate SiO $J = 1 - 0$ lines detection/non-detection, and variable types. The triangles on the upper side indicate the average color at each spectral type, derived from the sample in Paper I.

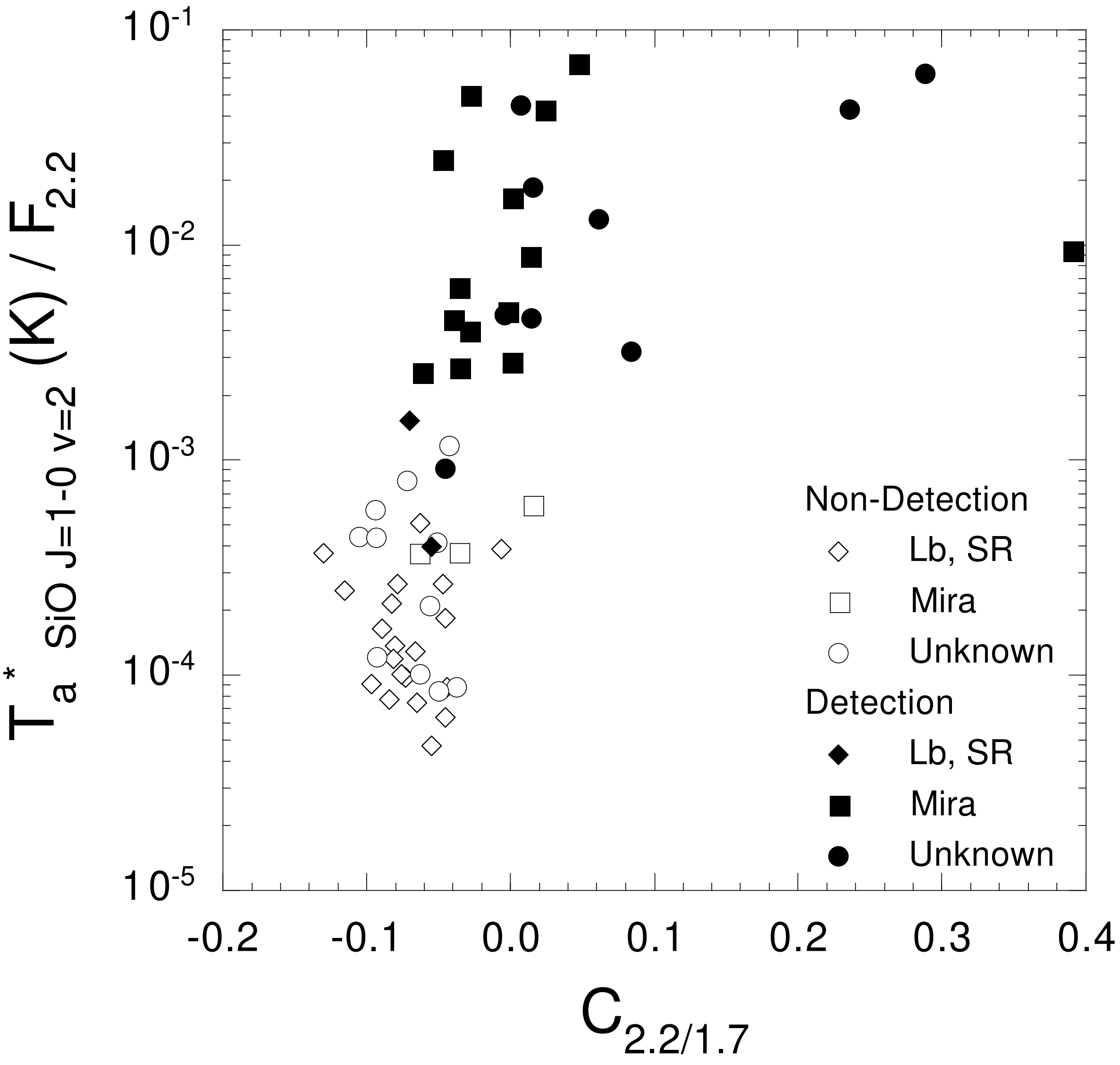

Fig.4. SiO $J = 1-0, v = 2$ maser intensity is plotted against $C_{12/2.2}$. For the non-detected stars, 3σ (1σ is the *rms* level) is used for maser intensity, and this indicates the upper limit. To make the parameter independent from the distance, SiO maser intensity is divided by $F_{2.2}$. $C_{12/2.2}$ is an indicator of the mass-loss rate. There is a correlation between these indices in low mass-loss rate stars ($C_{12/2.2} < 0.5$, approximate dust mass loss rate of 7×10^{-9} $M_\odot$ yr^{-1}).

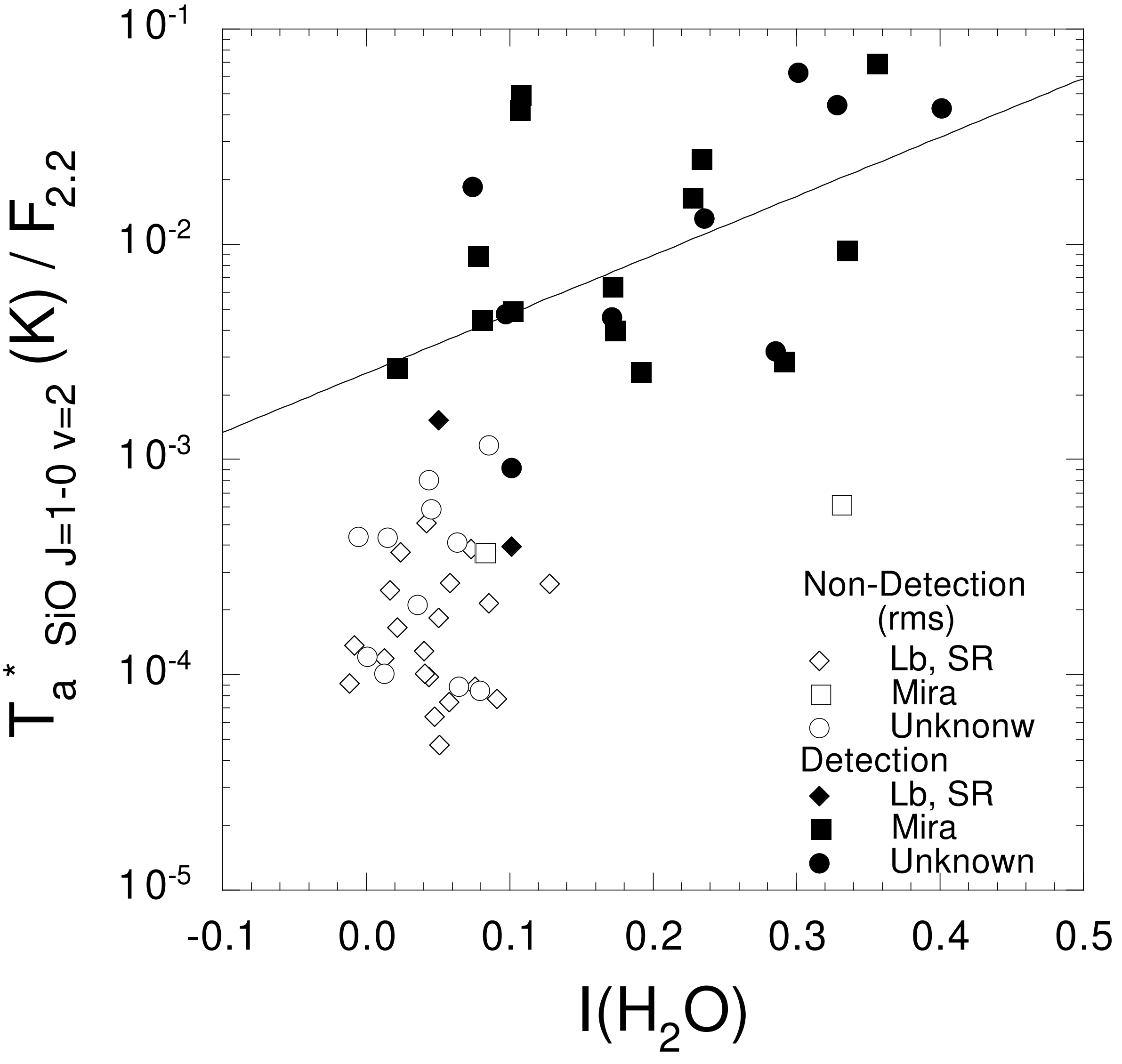

Fig.5. The relation between water index $I_{\mathrm{H_2O}}$ and SiO maser intensity is indicated. For non-detected sources, we use the 3 σ levels for T_{a}^*. Only a weak relation is seen between $I_{\mathrm{H_2O}}$ and SiO maser intensity.

Table 1. List of SiO $J = 1 - 0, v = 1$ and/or $v = 2$ masers detected sources.

IRAS name	R.A. (B.1950)	Dec (B.1950)	I_{H_2O}	$C_{2.2/1.7}$	GCVS name	Type	Comments
02255+6903 .	$02^{h}25^{m}33^{s}.8$	$+69^{d}03^{m}36^{s}.0$	0.074	0.015			
04081+5832 .	$04^{h}08^{m}06^{s}.8$	$+58^{d}32^{m}22^{s}.0$	0.171	0.015			
06266−1148 .	$06^{h}26^{m}36^{s}.1$	$-11^{d}48^{m}58^{s}.0$	0.286	0.084			
07019−1631 .	$07^{h}01^{m}58^{s}.0$	$-16^{d}31^{m}02^{s}.0$	0.328	0.007			
07232−0544 .	$07^{h}23^{m}13^{s}.0$	$-05^{d}44^{m}59^{s}.0$	0.234	−0.047	TT MON	M	1)
07268−0410 .	$07^{h}26^{m}52^{s}.0$	$-04^{d}10^{m}30^{s}.0$	0.022	−0.035	RX MON	M	
08186+1409 .	$08^{h}18^{m}36^{s}.6$	$+14^{d}09^{m}49^{s}.0$	0.172	−0.035	SZ CNC	M	
12341+5945 .	$12^{h}34^{m}07^{s}.0$	$+59^{d}45^{m}42^{s}.9$	0.192	−0.060	T UMA	M	
18076+3445 .	$18^{h}07^{m}37^{s}.0$	$+34^{d}45^{m}40^{s}.0$	0.301	0.288			
18156+0655 .	$18^{h}15^{m}40^{s}.8$	$+06^{d}55^{m}01^{s}.0$	0.228	0.002	BC OPH	M	
18186+3143 .	$18^{h}18^{m}37^{s}.6$	$+31^{d}43^{m}54^{s}.0$	0.101	−0.055	TU LYR	Lb	
18222+3933 .	$18^{h}22^{m}18^{s}.0$	$+39^{d}33^{m}24^{s}.0$	0.108	−0.027	TW LYR	M	1)
18347+2600 .	$18^{h}34^{m}45^{s}.0$	$+26^{d}00^{m}24^{s}.0$	0.081	−0.039	RZ HER	M	
18394+2845◇	$18^{h}39^{m}29^{s}.9$	$+28^{d}45^{m}56^{s}.4$	0.050	−0.070	SY LYR	SRb	
18561+1642 .	$18^{h}56^{m}10^{s}.0$	$+16^{d}42^{m}48^{s}.0$	0.174	−0.028	EU AQL	M	2)
19090+1746 .	$19^{h}09^{m}03^{s}.6$	$+17^{d}46^{m}48^{s}.0$	0.108	0.024	KK SGE	M	2)
19158+1955 .	$19^{h}15^{m}48^{s}.9$	$+19^{d}55^{m}54^{s}.0$	0.103	−0.001	NO SGE	M	2)
19172+1706 .	$19^{h}17^{m}18^{s}.0$	$+17^{d}06^{m}48^{s}.0$	0.292	0.001	W SGE	M	2)
19285+4853 .	$19^{h}28^{m}33^{s}.9$	$+48^{d}53^{m}45^{s}.0$	0.101	−0.046			
19308+0609◇	$19^{h}30^{m}55^{s}.0$	$+06^{d}09^{m}30^{s}.0$	0.059	−0.079	V 621AQL	SRb	
19412+0337 .	$19^{h}41^{m}15^{s}.3$	$+03^{d}37^{m}15^{s}.0$	0.402	0.236	*		
19550−0201 .	$19^{h}55^{m}01^{s}.0$	$-02^{d}01^{m}12^{s}.0$	0.357	0.048	RR AQL	M	
20077−0625 .	$20^{h}07^{m}46^{s}.0$	$-06^{d}24^{m}42^{s}.0$	0.336	0.392	V1300AQL†	M:	1)
20215+6243 .	$20^{h}21^{m}32^{s}.3$	$+62^{d}43^{m}21^{s}.0$	0.097	−0.004			
20234−1357 .	$20^{h}23^{m}26^{s}.0$	$-13^{d}57^{m}51^{s}.0$	0.236	0.061			
20296−2151 .	$20^{h}29^{m}38^{s}.7$	$-21^{d}51^{m}40^{s}.0$	0.332	0.016	RU CAP	M	
20305+6246 .	$20^{h}30^{m}35^{s}.4$	$+62^{d}46^{m}28^{s}.0$	0.078	0.014	BF CEP	M	

◇ indicates tentative detection. 'Type' is variable type according to GCVS. 'M' : Mira variable. 'SR' : semi-regular variable, 'SRb' : a sub-class of 'SR' and indicate semi-regular variable with 'poor defined periodicity'. 'Lb' : irregular variable. Comments show the quality of NIRS spectra. 1) Confusion with other source occurred, i.e more than 2 source entered in the one field of view when the star was observed, because of the NIRS's large aperture. Brightness of the fainter sources are about 20% of the target star at 2.2 μm. 2) The flux quality is low, because of the different satellite operation near the galactic plane. About 10 – 20 % flux uncertainty remains.

* IRC+00450 † IRC−10529

Table 2. List of SiO non-detected sources.

IRAS name	R.A. (B.1950)	Dec (B.1950)	$I_{\mathrm{H_2O}}$	$C_{2.2/1.7}$	GCVS name	Type	Comments
01010+7434	$01^{h}01^{m}03^{s}.8$	$+74^{d}34^{m}00^{s}.1$	0.013	−0.063			
01584+7103	$01^{h}58^{m}26^{s}.8$	$+71^{d}03^{m}24^{s}.0$	−0.005	−0.105			
03478+6349	$03^{h}47^{m}53^{s}.3$	$+63^{d}49^{m}13^{s}.0$	0.083	−0.035	BF CAM	M:	
04265+5718	$04^{h}26^{m}31^{s}.9$	$+57^{d}18^{m}12^{s}.7$	0.044	−0.073	RV CAM	SRb	
04554+4437	$04^{h}55^{m}29^{s}.8$	$+44^{d}37^{m}07^{s}.0$	0.063	−0.051			
05026+4447	$05^{h}02^{m}38^{s}.5$	$+44^{d}47^{m}40^{s}.0$	0.065	−0.037			
05176+3502	$05^{h}17^{m}35^{s}.0$	$+35^{d}02^{m}24^{s}.0$	0.073	−0.007	EE AUR	Lb	
06153−3100	$06^{h}15^{m}23^{s}.9$	$-31^{d}00^{m}14^{s}.6$	0.083	−0.063	EH CMA	M	
07186−1017	$07^{h}18^{m}36^{s}.2$	$-10^{d}17^{m}03^{s}.0$	0.128	−0.047	V 632MON	SR:	
07393−0403	$07^{h}39^{m}18^{s}.5$	$-04^{d}03^{m}30^{s}.0$	0.036	−0.056			
08196+1509	$08^{h}19^{m}36^{s}.9$	$+15^{d}09^{m}11^{s}.1$	0.041	−0.076	Z CNC	SRb	
11538+5808	$11^{h}53^{m}54^{s}.0$	$+58^{d}09^{m}00^{s}.0$	0.058	−0.065	Z UMA	SRb	
16418+5459	$16^{h}41^{m}52^{s}.0$	$+54^{d}59^{m}48^{s}.0$	0.051	−0.055	S DRA	SRb	
16473+5753	$16^{h}47^{m}24^{s}.0$	$+57^{d}54^{m}00^{s}.0$	0.091	−0.085	AH DRA	SRb	
17359+4555	$17^{h}35^{m}56^{s}.3$	$+45^{d}55^{m}58^{s}.0$	0.044	−0.072			
17473+4542	$17^{h}47^{m}22^{s}.0$	$+45^{d}42^{m}54^{s}.0$	0.013	−0.081	V 337HER	SRb	
18052+4326	$18^{h}05^{m}17^{s}.1$	$+43^{d}26^{m}40^{s}.4$	0.001	−0.093			
18064+4212	$18^{h}06^{m}26^{s}.0$	$+42^{d}12^{m}54^{s}.0$	0.041	−0.067	V529 HER	SR	
18291+3836	$18^{h}29^{m}11^{s}.0$	$+38^{d}36^{m}12^{s}.0$	0.017	−0.115	KP LYR	SR	
18401+2854	$18^{h}40^{m}07^{s}.0$	$+28^{d}54^{m}30^{s}.0$	0.076	−0.044	FI LYR	SRb	
18505+3327	$18^{h}50^{m}30^{s}.6$	$+33^{d}27^{m}29^{s}.0$	0.042	−0.063	HM LYR	Lb	
18512+3034	$18^{h}51^{m}12^{s}.8$	$+30^{d}34^{m}08^{s}.0$	0.085	−0.043			
19040+2416	$19^{h}04^{m}03^{s}.3$	$+24^{d}16^{m}32^{s}.0$	0.015	−0.093			
19194+1734	$19^{h}19^{m}28^{s}.2$	$+17^{d}34^{m}14^{s}.0$	0.048	−0.045	T SGE	SRb	2)
19267+0345	$19^{h}26^{m}43^{s}.0$	$+03^{d}45^{m}30^{s}.0$	0.051	−0.046	V 858AQL	Lb	
19306+0455	$19^{h}30^{m}39^{s}.0$	$+04^{d}55^{m}12^{s}.0$	−0.012	−0.097	V1293AQL	SRb	
19461+0334	$19^{h}46^{m}07^{s}.0$	$+03^{d}34^{m}18^{s}.0$	0.022	−0.090	WX AQL	SRb	
20073−1041	$20^{h}07^{m}22^{s}.5$	$-10^{d}41^{m}04^{s}.6$	0.046	−0.094	†		
20094−1121	$20^{h}09^{m}29^{s}.3$	$-11^{d}21^{m}21^{s}.1$	0.079	−0.050			
20161−1600	$20^{h}16^{m}08^{s}.0$	$-16^{d}00^{m}54^{s}.0$	0.085	−0.083	AE CAP	SR	
20311−2325	$20^{h}31^{m}11^{s}.0$	$-23^{d}25^{m}18^{s}.0$	0.024	−0.130	AK CAP	Lb	
22073+7231	$22^{h}07^{m}23^{s}.0$	$+72^{d}31^{m}24^{s}.0$	−0.008	−0.081	DM CEP	Lb	

Comment 2) means the same as table 1.

† SAO 163310

Table 3. Results of SiO maser observations for detected sources.

IRAS name	Date	$J=1-0, v=1$				$J=1-0, v=2$				$J=2-1, v=1$			
		rms	$V_{\rm LSR}$	$T_{\rm a}^*$	$S_{\rm a}^*$	rms	$V_{\rm LSR}$	$T_{\rm a}^*$	$S_{\rm a}^*$	rms	$V_{\rm LSR}$	$T_{\rm a}^*$	$S_{\rm a}^*$
02255+6903	5.20	0.04	−29.7	0.78	2.19	0.04	−28.9	0.92	3.16	0.07	−31.1	0.35	0.64
04081+5832	5.20	0.02	−111.9	0.15	0.47	0.02	−112.9	0.10	0.34	·	·	·	·
06266−1148	6.11	0.02	16.9	0.23	0.55	0.02	18.6	0.09	0.19	0.05	17.7	0.65	1.16
07019−1631	6.12	0.04	53.7	1.10	3.24	0.03	55.4	1.76	6.33	0.06	54.0	0.25	0.41
07232−0544	5.20	0.04	43.5	3.59	6.29	0.04	42.1	3.05	6.13	0.07	41.7	0.79	1.58
07268−0410	5.20	0.04	103.6	0.43	0.74	0.04	105.6	0.22	0.75	·	·	·	·
08186+1409	6.11	0.03	−36.0	0.31	0.10	0.03	−38.3	0.23	0.90	0.04	·	·	·
12341+5945	5.21	0.02	−83.3	0.10	0.38	0.02	−89.0	0.17	0.33	·	·	·	·
18076+3445	5.23	0.04	4.1	1.40	3.67	0.04	2.7	1.03	4.41	0.06	3.2	0.26	0.65
18156+0655	6.10	0.16	37.4	0.97	1.85	0.15	37.3	1.20	2.00	·	·	·	·
18186+3143(a)	5.22	0.03	·	·	·	0.03	·	·	·	0.05	19.1	0.37	1.97
18186+3143(b)	5.23	0.03	·	·	·	0.03	8.0	0.11	0.32	0.04	4.7	0.35	1.76
18186+3143(c)	6.11	0.03	·	·	·	0.03	5.6	0.14	0.61	0.05	8.4	0.24	·
18222+3933	5.23	0.04	18.9	7.95	20.04	0.04	20.6	6.07	31.42	0.06	17.9	4.04	14.15
18347+2600	5.24	0.03	55.7	0.24	0.85	0.03	57.3	0.19	0.58	0.05	·	·	·
18394+2845	5.24	0.04	·	·	·	0.04	−7.5	0.20	0.65	·	·	·	·
18561+1642	5.25	0.04	73.9	0.34	0.94	0.04	76.4	0.27	1.22	·	·	·	·
19090+1746	6.10	0.10	46.0	0.79	1.40	0.10	46.2	1.25	3.66	·	·	·	·
19158+1955	6.11	0.03	49.0	0.14	0.61	0.03	49.4	0.27	0.75	0.06	·	·	·
19172+1706	5.23	0.04	−54.7	0.32	0.91	0.03	−54.2	0.20	0.38	0.06	−54.5	0.39	1.40
19285+4853	5.24	0.05	12.0	0.34	0.88	0.04	11.2	0.13	0.39	0.17	·	·	·
19308+0609	5.24	0.04	46.6	0.17	0.17	0.03	·	·	·	0.14	·	·	·
19412+0337	5.23	0.08	−31.1	2.76	11.06	0.07	−31.5	2.01	8.01	0.12	−30.8	2.42	9.97
19550−0201	5.23	0.09	27.7	89.96	180.57	0.08	28.8	43.45	153.45	0.13	30.7	4.99	16.29
20077−0625	5.23	0.05	−18.2	0.42	0.93	0.05	−18.2	0.72	3.34	0.07	·	·	·
20215+6243	5.20	0.18	17.2	0.88	0.81	0.07	18.9	0.42	1.66	0.04	·	·	·
20234−1357	6.11	0.05	−33.3	1.90	6.78	0.05	−33.1	0.88	3.89	0.10	−32.1	0.98	1.90
20296−2151	6.10	0.04	6.4	0.66	0.73	0.03	·	·	·	·	·	·	·
20305+6246	6.11	0.04	−14.9	0.85	1.66	0.03	−14.5	1.19	3.55	0.07	−15.1	0.22	0.37

Date is observed day in M.DD. *Rms* is root mean square of the antenna temperature (K), $V_{\rm LSR}$ is velocity at intensity peak (km s^{-1}), $T_{\rm a}^*$ is antenna temperature at peak (K), $S_{\rm a}^*$ is integrated intensity (K km s^{-1}).

Table 4.a. The results of SiO maser observations for non-detected sources.

IRAS name	Date	$J=1-0, v=1$ rms	$J=1-0, v=2$ rms	$J=2-1, v=1$ rms
01010+7434	5.20	0.03	0.03	0.05
01584+7103	6.11	0.03	0.03	0.07
03478+6349	6.11	0.03	0.03	0.05
04265+5718	5.20	0.03	0.03	0.04
04265+5718	6.12	0.03	0.03	0.05
04554+4437	6.12	0.03	0.03	0.04
05026+4447	5.20	0.03	0.03	0.05
05026+4447	6.12	0.02	0.02	0.04
05176+3502	5.20	0.04	0.04	0.08
06153−3100	6.12	0.04	0.04	0.07
07186−1017	6.12	0.03	0.03	0.04
07186−1017	6.11	0.03	0.03	0.05
07393−0403	5.20	0.03	0.03	0.06
08196+1509	6.12	0.02	0.02	0.04
08196+1509	5.21	0.03	0.03	0.05
11538+5808	5.21	0.03	0.03	0.05
16418+5459	5.23	0.03	0.03	0.05
16473+5753	5.23	0.03	0.03	0.05
17359+4555	5.24	0.05	0.05	·
17473+4542	5.23	0.03	0.03	0.05
18052+4326	5.22	0.03	0.03	0.05
18064+4212	5.23	0.04	0.04	0.07
18064+4212	5.22	0.04	0.04	0.07
18291+3836	5.23	0.03	0.03	0.06
18291+3836	6.11	0.06	0.07	·
18401+2854	6.11	0.04	0.04	0.08
18401+2854	5.23	0.03	0.03	0.07
18505+3327	6.11	0.04	0.04	0.09
18512+3034	5.25	0.07	0.07	·
19040+2416	5.23	0.04	0.03	0.06
19194+1734	6.10	0.05	0.05	·
19267+0345	5.24	0.03	0.03	0.06
19267+0345	6.10	0.03	0.03	·

rms (root mean square) is in the unit of K.

Table 4.b. *Continued.*

IRAS name	Date	$J=1-0, v=2$ rms	$J=1-0, v=1$ rms	$J=2-1, v=1$ rms
19306+0455	5.24	0.03	0.03	0.06
19461+0334	5.24	0.03	0.03	0.09
19461+0334	5.23	0.04	0.04	0.06
20073−1041	5.23	0.04	0.03	0.06
20094−1121	5.24	0.03	0.03	0.07
20161−1600	5.24	0.03	0.03	0.06
20161−1600	6.11	0.03	0.03	0.06
20311−2325	5.23	0.03	0.02	0.05
22073+7231	5.20	0.03	0.03	0.05
22073+7231	6.11	0.03	0.03	0.08

Table 5. The distribution of detected source and non-detected source at each variable type.

Type	Detected	Non-detected
Mira	15	2
SR	2	14
Lb	1	5
Unknown	9	11
Total	27	32

Table 6. The observations of near-infrared water spectra and SiO masers.

Name		Type	$N(H_2O)$ cm^{-2}	$T_{ex}(H_2O)$ K	SiO Masers			d (pc)	ref.
					J=1-0	J=1-0	J=2-1		
					$v = 1$	$v = 2$	$v = 1$		
AK Cap	....	Lb	5×10^{19}	1000–1500	N	N	N	497	Paper I, this work
SAO 163310	....	·	1×10^{20}	1000–1500	N	N	N		Paper I, this work
V Hor	....	SRb	1×10^{20}	1000–1500	N			336	Paper I, (4)
β Peg	....	Lb	7×10^{18}	1250	N	N		61	(1), (5)
g Her	....	SRb	2×10^{19}	1250	N	N		111	(1), (5)
SW Vir	....	SRb	3×10^{19}	1250	N	N	D	143	(1), (5), (6)
R Leo	warm	Mira	$< 5 \times 10^{19}$–3×10^{20}	1700	D		D	101	(2), (7), (8)
	cool		2×10^{21}–2×10^{22}	1150 – 1200					
o Cet	hot	Mira	3×10^{21}	2000	D		D	128	(3), (8), (9)
	cool		3×10^{20}	1400					
Z Cas	hot	Mira	3×10^{21}	2000					(3), (10)
	cool		1×10^{21}	1200					

'd' indicates the distance to the star from the Hipparcos and Tycho catalogues (1997). Hinkle & Barnes (1979) and Yamamura et al. (1999b) measured water spectra with two components of layers, and both layers are indicated individually. The phase dependence of density and temperature is detected in R Leo. In the column in SiO maser, D is detection and N is non-detection. References (1)–(3) are for the water observations and reference (4)–(10) are for the SiO maser observations.

(1) Tsuji et al. (1997)

(2) Hinkle & Barnes (1979)

(3) Yamamura et al. (1999b)

(4) Allen et al. (1989)

(5) Alcolea et al. (1990)

(6) Herpin et al. (1998)

(7) Heske (1989)

(8) Nyman & Olofsson (1986)

(9) Buhl et al. (1974)

(10) Spencer et al. (1981)